Final Report

August 7, 1992

Effects of Convection Electric Field on Upwelling and Escape of Ionospheric O^+

Contract NAS5-31211

Customer: NASA Goddard Space Flight Center
Greenbelt, MD 20771

Principal Investigator: J. B. Cladis
Co-investigators:
Yam T. Chiu and William K. Peterson

Space Sciences Laboratory
Lockheed Palo Alto Research Laboratory
3251 Hanover Street
Palo Alto, CA 94304

NASA
National Aeronautics and Space Administration

Report Documentation Page

1. Report No.	2. Government Accession No.	3. Recipient's Catalog No.

4. Title and Subtitle
Effects of Convection Electric Field on Upwelling and Escape of Ionospheric O^+

5. Report Date
August 7, 1992

6. Performing Organization Code

7. Author(s)
J.B. Cladis, Y.T. Chiu and W.K. Peterson

8. Performing Organization Report No.

10. Work Unit No.

9. Performing Organization Name and Address
Lockheed Palo Alto Research Laboratory
3251 Hanover Street
Palo Alto, CA 94304

11. Contract or Grant No.
NAS5-31211

13. Type of Report and Period Covered
Final Report 5/7/91-8/7/92

12. Sponsoring Agency Name and Address
NASA Goddard Space Flight Center

14. Sponsoring Agency Code

15. Supplementary Notes

16. Abstract

SEE ATTACHED SHEET

17. Key Words (Suggested by Author(s))	18. Distribution Statement
Upwelling Ions, Ion Acceleration, Ion Transport, Convection Electric Field Collisional Effects, Ionosphere	Unclassified - Unlimited

19. Security Classif. (of this report)	20. Security Classif. (of this page)	21. No. of pages	22. Price
Unclassified	Unclassified	4	

NASA FORM 1626 OCT 86

ABSTRACT

A Monte Carlo code is used to explore the full effects of the convection electric field on distributions of upflowing O^+ ions from the cusp/cleft ionosphere. Trajectories of individual ions/neutrals are computed as they undergo multiple charge-exchange collisions. In the ion state, the trajectories are computed in realistic models of the magnetic field and the convection, corotation, and ambipolar electric fields. The effects of ion-ion collisions are included, and the trajectories are computed with and without simultaneous stochastic heating perpendicular to the magnetic field by a realistic model of broadband, low frequency waves. In the neutral state, ballistic trajectories in the gravitational field are computed. The initial conditions of the ions, in addition to ambipolar electric field and the number densities and temperatures of O^+, H^+, and electrons as a function of height in the cusp/cleft region were obtained from the results of Gombose and Killeen [1987], who used a hydrodynamic code to simulate the time-dependent frictional-heating effects in a magnetic tube during its motion though the convection throat. The distribution of the ion fluxes as a function of height are constructed from the case histories.

The results show that during disturbed times, with a cross polar-cap potential equal to 100 kV in the Heppner-Maynard convection-potential model, a high flux ($> 10^8$ $cm^{-2}s^{-1}$ at 1000 km) of low-energy O^+ ions flow outward from the ionosphere. At the altitude of 20,000 km, these ions reach energies approaching 15 eV and their pitch-angle distributions become very narrow (half-width $\approx 5°$). If these ions enter the region in which the broadband, low-frequency wave field is present, they become heated; their energies increase and their pitch-angle distribution broadens during this process. Experimental observations of both these types of upflowing ions are discussed.

A further result is that the very strong electric fields perpendicular to the magnetic field in cusp/cleft auroral structures that were reported by Sugiura et al. [1984], Sandholt [1988], and Sandholt et al. [1989a; 1989b] can directly accelerate O^+ions from the ionosphere, even in the absence of the heating and diffusion processes. An ion with an intial energy of 0.6 eV and pitch-angle of 45° at 2000 km is accelerated to 105 eV at 20,000 km if it remains within magnetic field lines, assumed to be equipotentials, that produce a transverse electric field of 0.25 V/m at 300 km.

I. INTRODUCTION

O^+ ions, among other species, regularly flow outward from the ionosphere in region of the dayside cusp/cleft. The processes responsible for the outflow of these ions are of great interest because, as discussed by Cladis [1986], these ions enter the magnetosphere in the region where they may subsequently become appreciably accelerated by the convection electric field and transported to the near magnetotail. The pressure of these ions in the magnetotail, which was computed recently by Cladis and Francis [1992], suggests that these ions may trigger a substorm through the development of velocity shear instabilities. Moreover, during disturbed times, these ions often supply the major energy content of the ring current [Cladis and Francis, 1985; Horwitz, 1987; Delcourt et al. 1990].

Various wave-particle interactions [Chiu et al., 1989; Crew et al., 1990, and references therein] have been proposed to explain the ionic outflow from this region, and some of these interactions may indeed be responsible for the more energetic conics that are observed at high altitudes. However, the convection electric field, which is particularly strong in the convection throat, may be principally responsible for the outflow of these ions by accelerating them to higher altitudes where they may be further accelerated by other processes. Such a prominent role for the convection electric field is indicated by the correlation of the ionic outflux with indices of enhanced ionospheric convection [Lockwood et al, 1985; Yau and Lockwood, 1988; Yau et al. 1988]. Also, the escape flux is accompanied at lower altitudes ($< 2\ R_E$) with the so-called upwelling ions — ions of various species (He^+, O^+, N^+, NO^+ and O^{++}, but mainly O^+) — that move upward with velocities of several km/s. This general upwelling of ionized atoms and molecules indicates the action of a strong ionospheric heating process. Moreover, hydrodynamic calculations of the frictional heating of ions in a magnetic tube convected through the throat have reproduced several features of the upwelling ions. The results of Gambosi and Killeen [1987] obtained with a time-dependent hydrodynamic code are particularly promising.

In the research described here, an ion transport code is used to extend the hydrodynamic calculations to high altitudes in the magnetosphere. Hydrodynamic codes do not properly handle non-Maxwellian plasmas or the acceleration and expansion of ion distributions into the magnetosphere. Moreover, the transport code includes the following additional processes whereby the convection electric field affects the motion of the ions:

(1) The outward acceleration of ions, along the magnetic field, by the Coriolis force evoked by $\vec{V}_E$, the $\vec{E} \times \vec{B}$ drift of the ions. Cladis [1986] has shown that at altitudes higher than a few $R_E$this is the dominant force that acts on upflowing ions from the ionosphere.

(2) Energy diffusion due to collisions of the ions with neutrals and ions in the presence of the convection electric field. The hydrodynamic codes compute this Joule (frictional) heating, which is very important at altitudes less than about 500 km. But the process is also important at higher altitudes where the anisotropy of the ions must be taken into account.

(3) Effects of multiple charge-exchange collisions. Owing to the divergence of the magnetic field, ions can acquire high upward velocity components through multiple exchange collisions. The convection electric field, which on the average maintains the perpendicular velocity components of the ions at nearly the same level, effectively pumps energy into the parallel component. Intervening momentum-transfer collisions, together with the actions of the $\mu\nabla_{\parallel}B$ force and the ambipolar electric field enhance the outward velocity of the ions.

(4) Wave-ion interactions. The convective flow in the throat region is susceptible to shear instabilities that result in magnetic and electric field turbulence [e.g., Kintner, 1976]. Ions can be accelerated stochastically by temporal and spatial fluctuations comparable with the ion gyroperiod and gyroradius, respectively, in the frame of the drifting ions.

The ion-transport properties are constructed from case histories computed with a Monte-Carlo type code. The Monte Carlo code follows individual ions/neutrals as they undergo multiple (up to 4) charge-exchange collisions. In the ion state, the trajectories are computed in realistic models of the magnetic field and the convection, corotation, and ambipolar electric fields. Moreover, stochastic effects due to ion-ion collisions and wave-particle interactions are included. In the neutral state, ballistic trajectories in the gravitational field are computed.

The results show that during disturbed times, with a cross polar-cap potential equal to 100 kV in the convection-potential model of Heppner and Maynard [1987], a high flux ($> 10^8$ $cm^{-2}s^{-1}$ at 1000 km) of low-energy O^+ ions flow outward from the ionosphere. At the altitude of 20,000 km, these ions reach energies approaching 10 eV and their pitch-angle distributions become very narrow (half-width $\approx 5°$). Here, these ions are referred to as "unheated", because they have not been heated by the intense broadband, low-frequency wave field that is often present on auroral field lines [Gurnett and Frank, 1977; Gurnett et al., 1984]. If these ions enter the region in which the waves are present, they become heated; their energies increase and their pitch-angle distribution broadens during this process. Both these types of upflowing ions have been observed.

A further result is that the very strong electric fields perpendicular to the magnetic field in cusp/cleft auroral structures that were reported by Sugiura et al. [1984], Sandholt [1988], and Sandholt et al. [1989a; 1989b] can directly accelerate O^+ions from the ionosphere, even in the absence of the heating and diffusion processes. An ion with an intial energy of 0.6 eV and pitch-angle of 45° at 2000 km is accelerated to 105 eV at 20,000 km if it remains within magnetic field lines, assumed to be equipotentials, that produce a transverse electric field of 0.25 V/m at 300 km.

II Transport Calculations

1. Computer Codes

The Monte Carlo code used in this research was principally constructed of codes we had previously developed to compute the transport of ions in the magnetosphere [Cladis and Francis, 1992, 1985; Cladis, 1986; Cladis, 1988] and in the ionosphere [Chiu et al., 1988]. The former (magnetospheric) codes compute either the guiding-center motion or the full gyration motion of ions in prescribed models of the geomagnetic and geoelectric fields and contains options to compute simultaneously the stochastic acceleration of ions due to a specified distribution of transverse electric field variations. The latter (ionospheric) codes simulate ion heating and multiple charge-exchange effects in the auroral ionosphere. Trajectories of multiple charge-exchange events are computed by following atoms both in their charged state (guiding-center motion) and neutral state (ballistic motion) as they repeatedly gain and lose charge. A probabilistic test at each Δt is conducted to determine whether a charge exchange reaction had occurred. Periodic boundary conditions are assumed, i.e., particles that move across a boundary of the convecting magnetic tube are reinjected with the same velocity space characteristics at complementary configuration space locations in the tube.

Additional codes were added to compute the effects of ion-neutral and ion-ion collisions. The ion-neutral collisions code accounts for elastic, inelastic, and charge-exchange collisions of O^+on ambient O atoms; charge-exchange collisions of O^+on ambient H atoms; elastic and inelastic collisions of energetic O (from O^+on O charge-transfer events) on ambient O atoms; and charge-exchange collisions of energetic O atoms with ambient $O^+$and ambient H^+. Here, 'ambient' refers to the initial distribution of a specie in the tube. Between collisions the ion motion is assumed to be adiabatic; the ion is moved along and across the magnetic field by integrating the equations of the guiding-center motion described by Northrop [1963] (see Cladis [1988]). The collision probability is determined as described by Cladis and Francis [1985]. Since the ion-neutral collision time is much longer than the ion gyrofrequency, the velocity vector of an ion prior to a collision is determined by a uniform sampling (0° to 360°) of the ion gyrophase. The scattering angles appropriate for the particular collision are also randomly selected, and the calculation is resumed starting with the new velocity vector.

Since the ion-ion collision frequency is very high, a stochastic process is used to determine the diffusion of the ions. This process is described in the following subsection.

1.1 Ion-Ion Collisions

The diffusion of O^+ due to ion-ion collisions is based on the diffusion coefficients derived by Chandrasekhar [1942] and Spitzer [1956]. Three coefficients are used: $< (\delta v_d) >$, $< (\delta v_s)^2 >$, and $< (\delta v_p)^2 >$. Here, $< (\delta v_d) >$, the coefficient of dynamical friction, is the rate at which the test particles (the traced ions) are slowed down by collision with the field

particles (O^+ ions of the ambient plasma); $< (\delta v_s)^2 >$ is rate of increase of $(\Delta v)^2$ in the direction parallel to the initial direction of motion of the test particles; and $< (\delta v_p)^2 >$ is the rate of increase in the direction perpendicular to the initial direction of the test particles.

$$< (\Delta v_d) >= -\frac{2A_D}{V_{th}^2} G(V/V_{th}) \tag{1}$$

$$< (\Delta v_s)^2 >= \frac{A_D}{V} G(V/V_{th}) \tag{2}$$

$$< (\Delta v_p)^2 >= \frac{A_D}{V} [\Phi(V/V_{th}) - G(V/V_{th})] \tag{3}$$

where

$$A_D = \frac{8\pi e^4}{m^2} n(O^+) \ln\Lambda \tag{4}$$

$\Phi(x)$ is the error function,

$$\Phi(x) = \frac{2}{\sqrt{\pi}} \int_0^x \exp(-t^2) dt \tag{5}$$

and

$$G(x) = \frac{\Phi(x) - x\Phi'(x)}{2x^2} \tag{6}$$

where the prime denotes the derivative with respect to x. Additionally, V is the ion speed, V_{th} is the thermal speed ($\sqrt{2kT/m}$), e is the unit charge (4.8×10^{-10} esu), and

$$\Lambda = \frac{1.5}{e^3} \left(\frac{k^3 T_1 T^2}{\pi n_e} \right)^{\frac{1}{2}} \tag{7}$$

Here, T_1 and T are the temperature of the field ions and the test-particle ions, respectively, and n_e is the electron number density. In the region where the ion-ion collisions are important, $T_1 \approx T$ and $n_e \approx n(O^+)$.

As described above, the motion of an ion is assumed to be adiabatic during the time interval Δt between collisions. At the end of the time interval, the ion velocity vector in the $\vec{V}_E$ frame is altered by the velocity increments δv_d, δv_s, and δv_p, arising from the coefficients $< (\Delta v_d) >$, $< (\Delta v_s)^2 >$, and $< (\Delta v_p)^2 >$, respectively. Here,

$$\delta v_d =< (\Delta v_d) > \Delta t \tag{8}$$

and the velocity increments δv_s and δv_p are determined probabilistically as follows:

The distributions of δv_k, where the subscript k stands for s or p, are assumed to be Gaussian,

$$P(\delta v_k) = \frac{1}{\sqrt{2\pi}\sigma_k} \exp\left[-\frac{(\delta v_k)^2}{2\sigma_k^2} \right] \tag{9}$$

where

$$\sigma_k^2 = 2\delta t < (\Delta v_k)^2 > \tag{10}$$

Then a random number Q, uniformly distributed between 0 and 1, is selected and equated to the cummulative probability integral,

$$Q = \int_{-\infty}^{\xi} P(y)dy \tag{11}$$

where $y = \frac{\delta v_k}{\sqrt{2}\sigma_k}$. After solving (11) for ξ, the velocity increment is given by

$$\delta v_k = \sqrt{2}\sigma_k \xi \tag{12}$$

Note that δv_k may be positive or negative.

The increments δv_d and δv_s, which alter the **magnitude** of the velocity vector, alter the parallel and perpendicular velocity components, $V_\parallel$ and $V_\perp$, by the amounts $(\delta v_d + \delta v_s)\cos\alpha$ and $(\delta v_d + \delta v_s)\sin\alpha$, respectively. The increment δv_p changes both the pitch angle α and the guiding-center position perpendicular to $\vec{B}$. Since the direction of δv_p is distributed uniformly in azimuth about $\vec{V}$, the average rms value of δv_p along two orthogonal axes normal to $\vec{V}$ is $\delta v_p/\sqrt{2}$. Hence, by taking one of these axes to be in the plane of $\vec{V}_\parallel$ and $\vec{V}_\perp$, it is clear that the pitch-angle change will be

$$\delta\alpha \approx \frac{1}{\sqrt{2}}\frac{\delta v_p}{V} \tag{13}$$

And the increment along the axis normal to the $\vec{V}_\parallel$, $\vec{V}_\perp$ plane changes the guiding-center position by

$$\delta r = \frac{1}{\sqrt{2}}\frac{\delta v_p}{\Omega} \tag{14}$$

where Ω is the angular gyrofrequency of the ion. Since any direction of $\delta\vec{r}$ about $\vec{B}$ is equally probable, it is taken to be at angle γ with respect to the convection electric field $\vec{E}_c$, where γ is randomly selected from the range 0 - 360°.

The change in the circular energy $(mV_\perp^2/2)$ of the ion due to the displacement of the guiding center along $\vec{E}_c$ is

$$\delta W_E = eE_c\delta r\cos\gamma \tag{15}$$

Hence, the change in $V_\perp$ due to δv_p is

$$(\delta V_\perp)_{\delta v_p} = V_\perp\left[\sqrt{1 + \frac{\delta W_E}{mV_\perp^2/2}} - 1\right] \tag{16}$$

Finally, by combining the effects of all the increments, the full alterations of $V_{\|}$ and $V_{\|}$ are given by the equations,

$$\delta V_{\|} = (\delta v_d + \delta v_s)\cos(\alpha + \delta\alpha) \tag{17}$$

and

$$\delta V_{\perp} = (\delta v_d + \delta v_s)\sin(\alpha + \delta\alpha) + V_{\perp}\left[\sqrt{1 + \frac{\delta W_E}{mV_{\perp}^2/2}} - 1\right] \tag{18}$$

In the equations above $V_{\perp}$ is limited to a small value > 0.

A restriction on the use of the probability distribution (9) is that σ_k be less than V. This condition can be assured if the time step Δt is taken to be sufficiently small such that

$$\Delta t < \frac{V^2}{2 < (\Delta v_k)^2 >} \tag{19}$$

A similar procedure is used to simulate energy diffusion due to wave-particle interactions. The distribution of the perpendicular energy increments is taken to be Gaussian with $\sigma = 2\Delta t D_{\perp\perp}$, where $D_{\perp\perp} = e^2 w_{\perp} P_{\nu}/(8m)$ is the diffusion coefficient and P_{ν} is related to the power spectral density of the waves. Here, too, there is a restriction on the magnitude of Δt, viz.,

$$\Delta t < \frac{w_{\perp}}{2D_{\perp\perp}} \tag{20}$$

[Cladis and Francis, 1985]. In the computer program, Δt is selected to satisfy the smallest of the limits given by (19) for k = s and k = p and (20).

2. Magnetospheric Models

The magnetosphere is modeled by (1) the "short-tail" version of the magnetic field model of Tsyganenko [1987], as improved and coded by David Stern of NASA/Goddard, with the model parameters set for $Kp \geq 5^-$ and tilt angle = 0°, and (2) the convection electric field model of Heppner and Maynard [1987] that is generally appropriate in the northern hemisphere for $(B_y)_{IMF} > 0$. The polar-cap potential drop, $\Delta\Psi$, is taken to be 100 kV, which is appropriate for $Kp \approx 5^-$ and AE $\approx$ 600 according to Table 1 of Heppner and Maynard [1987]. Therefore, the models used here are appropriate for more highly disturbed times. The vector sum of the corotation electric field and the convection electric field is mapped from the reference plane in the ionosphere, where the Heppner-Maynard convection potentials are specified, to the ion positions in the magnetosphere assuming the magnetic field lines to be equipotentials [Cladis and Francis, 1992]. For the neutral atmosphere, the model of Anderson and Francis [1966] is used.

As discussed in the Introduction, Gombose and Killeen [1987] used a hydrodynamic code to simulate the time-dependent frictional-heating effects in a magnetic tube during

its motion though the convection throat. These authors also simulated the effects of precipitating electrons, which principally affected their electron distribution. The number densities and temperatures of O^+, H^+, and the electrons as a function of height in the cusp/cleft region were obtained from their results for times greater than 5 minutes. These properties are used to evaluate the diffusion coefficients (Equations (1)-(3)), the O^+source used in the transport calculations, and the ambipolar electric field. The ambipolar electric field $E_a = -d\Psi_E/ds$ is evaluated by differentiating the equation,

$$n_e = n_o e^{e\Psi_E/kT_e} \tag{21}$$

assuming the electrons to have a Boltsmann distribution and the plasma to be quasineutral ($n_e \approx n_i$).

The power-spectral density of the waves is taken to be $P_\nu = 5.0\nu^{-\beta}$ $(mV/m)^2/Hz$, where ν is the wave frequency and $\beta = 0.857$. This is the electric-field wave power that was measured in the cusp/cleft region with the DE 1 satellite on March 7, 1984 [André et al., 1990]. It is assumed to be the same over the altitude range 2000 km to 20,000 km, as implied by the measurements of Gurnett et al. [1984]. Note that the wave power at the O^+gyrofrequency, which is used in the diffusion coefficient, increases with altitude as $B^{-\beta}$.

3. Construction of Ion Properties

The case histories of the traced ions are used to construct the following ion properties as a function of height: the directional flux $j(w,\alpha)$ in units of $cm^{-2}s^{-1}sr^{-1}eV^{-1}$, differential omnidirectional flux $dJ(w)/dw$ in units of $cm^{-2}s^{-1}eV^{-1}$, integrated flux F_{up} $(cm^{-2}s^{-1})$ parallel to $\vec{B}$, and number density n (cm^{-3}).

The ion flux $j_s(w,\alpha)$ at the source altitude is taken to be Maxwellian with a temperature of 2400°. Each of the traced ions l_{mn} represents a current of $\delta\dot{N}_{mn}$ ions per second moving upward along the magnetic field through a cross section δA_s normal to the magnetic field.

$$\delta\dot{N}_{mn} = \delta A_s \int_{w_{m-\frac{1}{2}}}^{w_{m+\frac{1}{2}}} j_s(w,\alpha)dw \int_{\alpha_{n-\frac{1}{2}}}^{\alpha_{n+\frac{1}{2}}} 2\pi sin\alpha cos\alpha d\alpha \tag{22}$$

Here, the energy limits are chosen to divide the ion current into 5 equal parts between the thermal energy and infinity, and the pitch-angle limits divide the current into 5 equal parts between 90° and 180°. (The ions are traced in the northern polar cap so ions in this pitch-angle interval move upward). The energies w_m and pitch-angles α_n at the mid-current values within the above intervals are the initial values of the traced ions l_{mn}. Twenty-five ions with the same initial conditions are traced. Since the number of different initial conditions is also 25, a total of 625 ions are traced.

The ion case histories are tallied in planes normal to $\vec{B}$ to a maximum altitude of 20,000 km. The listing for each ion that crosses a plane includes the trajectory number l, time, geographic position, energy, pitch-angle, and the magnetic and electric field components.

In each reference plane, ions are tallied in five energy bins and five pitch-angle bins , which have widths that depend on energy- and pitch angle- ranges of the ions that cross the plane. The directional flux at the energy w_k and pitch angle α_j is then given by the summation

$$j(w_k, \alpha_j) = \frac{\sum_{m,n} g_{mnkj}}{\delta A_p \pi(\cos^2\alpha_{j+\frac{1}{2}} - \cos^2\alpha_{j-\frac{1}{2}})\delta w_k} \tag{23}$$

Here, $g_{mnjk} = \delta \dot{N}_{mn}$ when the energy and pitch angle of the ion l_{mn} fall into the energy bin k and the pitch-angle bin j, respectively. Since the magnetic flux is conserved, the ratio of the areas $\delta A_s/\delta A_p$ is equated to the ratio of the average magnetic-field intensity in the plane to that at the source.

The other properties of the ions follow directly from the flux:

$$\frac{\delta J(w)}{\delta w_k} = \sum_j j(w_k, \alpha_j) 2\pi(\cos\alpha_{j+\frac{1}{2}} - \cos\alpha_{j-\frac{1}{2}}) \tag{24}$$

$$F_{up} = \sum_{j,k} j(w_k, \alpha_j)\pi(\cos^2\alpha_{j+\frac{1}{2}} - \cos^2\alpha_{j-\frac{1}{2}})\delta w_k \tag{25}$$

and

$$n_{up} = \sum_{j,k} \pi(cos^2\alpha_{j+\frac{1}{2}} - cos^2\alpha_{j-\frac{1}{2}}) \int_{w_{m-\frac{1}{2}}}^{w_{m+\frac{1}{2}}} \frac{dw}{\sqrt{2w/m}} \tag{26}$$

Preliminary computer runs were made to determine an appropriate altitude for the source altitude. It was found that at altitudes less than about 750 km, the change exchange rate appreciably reduced the outflux of O^+. Moreover, at altitudes up to about 1500 km, ion-ion collisions were very effective in keeping the ions thermalized. Therefore, the source altitude was taken to be 2000 km, and the ion properties were computed at the altitudes 4,000, 8,000, 12,000, 16,000, and 20,000 km.

III RESULTS

1. O^+ Distribution in Absence of Wave-Particle Interactions

First, the O^+properties were computed for the case in which wave-particle interactions were not present. Table 1 shows the average directional flux of these ions in the energy and pitch-angle bins at each altitude. Note that the energy of the ions increases toward increasing altitudes, although the energy does not exceed 14.7 eV., and that the flux is high, above 10^8 ions $cm^{-2}s^{-1}sr^{-1}eV^{-1}$, even at the altitude of 20,000 km. In Figure 1 the logarithm of the flux is depicted in $V_\perp$, $V_\parallel$ coordinates. Here, the bins are in velocity intervals corresponding to the energy and pitch-angle intervals. The scale in the figure gives the correspondence of the logarithm of the flux to the grey-tone shading. This figure

Table 1. Flux ($cm^{-2}s^{-1}sr^{-1}eV^{-1}$) of "unheated O^+ ions in velocity, pitch-angle bins at altitudes 4,000 to 20,000 km.

ALTITUDE = 4000 KM

Pitch-angles (deg) / Velocities (km/s)	110.55–124.33	124.33–138.11	138.11–151.90	151.90–165.68	165.68–179.46
0.399– 2.594	6.7461E+05	2.2265E+06	3.5236E+06	7.7706E+06	4.1961E+07
2.594– 3.647	1.0119E+06	1.9482E+06	8.8089E+06	1.8404E+07	8.0694E+07
3.647– 4.458	0.0000E+00	3.0615E+06	7.3407E+06	1.9222E+07	2.6898E+07
4.458– 5.142	0.0000E+00	1.3916E+06	5.2853E+06	4.0898E+06	1.0759E+06
5.142– 5.746	0.0000E+00	0.0000E+00	5.8726E+05	0.0000E+00	0.0000E+00

ALTITUDE = 8000 KM

Pitch-angles (deg) / Velocities (km/s)	159.53–163.61	163.61–167.69	167.69–171.77	171.77–175.85	175.85–179.93
3.931– 4.944	0.0000E+00	0.0000E+00	1.4597E+06	0.0000E+00	1.3947E+07
4.944– 5.782	0.0000E+00	3.1991E+06	8.7585E+06	3.7040E+07	2.4407E+08
5.782– 6.513	4.2682E+05	9.0642E+06	4.1603E+07	6.4522E+07	2.0223E+08
6.513– 7.170	8.5363E+05	1.7062E+07	1.4597E+07	1.0754E+07	6.9734E+06
7.170– 7.771	8.5363E+05	3.1991E+06	0.0000E+00	0.0000E+00	0.0000E+00

ALTITUDE = 12000 KM

Pitch-angles (deg) / Velocities (km/s)	169.22–171.37	171.37–173.53	173.53–175.69	175.69–177.84	177.84–180.00
4.233– 5.770	0.0000E+00	5.0925E+05	1.4175E+06	1.1762E+06	7.0266E+06
5.770– 6.977	3.9915E+05	2.5462E+06	1.1340E+07	4.5873E+07	2.0377E+08
6.977– 8.003	5.9873E+06	2.0879E+07	4.6778E+07	3.6463E+07	2.1783E+08
8.003– 8.912	1.5966E+06	6.1110E+06	4.2525E+06	1.5291E+07	1.7567E+07
8.912– 9.737	7.9830E+05	5.0925E+05	7.0876E+05	0.0000E+00	0.0000E+00

ALTITUDE = 16000 KM

Pitch-angles (deg) / Velocities (km/s)	173.22–174.58	174.58–175.93	175.93–177.29	177.29–178.64	178.64–180.00
5.410– 7.188	3.6557E+05	1.8742E+06	1.3087E+06	6.5298E+06	1.3011E+07
7.188– 8.605	2.9246E+06	3.7484E+06	5.8891E+06	1.5236E+07	4.8792E+07
8.605– 9.821	2.5590E+06	8.4340E+06	1.8976E+07	3.8090E+07	1.3662E+08
9.821–10.901	7.3115E+05	4.2170E+06	1.7013E+07	4.2443E+07	2.2770E+08
10.901–11.884	3.6557E+05	2.3428E+06	7.8521E+06	1.3060E+07	1.6264E+07

ALTITUDE = 20000 KM

Pitch-angles (deg) / Velocities (km/s)	175.33–176.26	176.26–177.20	177.20–178.13	178.13–179.07	179.07–180.00
7.018– 9.090	1.8170E+06	3.4992E+06	5.4374E+06	1.4490E+07	4.8885E+07
9.090–10.771	2.4226E+06	2.3328E+06	4.3499E+06	1.1773E+07	5.4316E+07
10.771–12.223	6.0566E+05	1.1664E+06	3.2624E+06	1.6301E+07	6.2464E+07
12.223–13.519	6.0566E+05	1.9440E+06	6.5249E+06	3.1696E+07	9.5053E+07
13.519–14.702	0.0000E+00	2.7216E+06	1.3593E+07	3.8941E+07	1.4394E+08

clearly shows that the pitch-angle distribution of the ions become narrower toward higher altitudes as the ions become more field aligned. It also shows that at each altitude the highest flux is at the smallest pitch angle, but at the higher velocities the distribution tends toward a conic, especially at altitudes below 16,000 km.

Histograms of the differential omnidirectional flux, dJ/dw, in the altitude planes are shown in Figure 2. Since this flux is obtained by integrating the directional flux over pitch-angle, its magnitude decreases with increasing energy. Note also that the peak of the energy spectrum moves toward the highest energy bin as the altitude increases. This effect is expected principally because the force $\vec{V}_E \cdot d\hat{e}/dt$, which accelerate ions along the magnetic field, has a component $V_\parallel \vec{V}_E \cdot d\hat{e}/ds$, which is proportional to the parallel velocity component of the ion. Here, $\hat{e}$ is a unit vector along the magnetic field and ds is an incremental distance along the local magnetic field line. The energy spectrum at 4000 km is roughly characterized by a temperature of about 0.45 eV.

Figure 3 shows the parallel flux (upper panel) and number density (lower panel) of the ions as a function of height. In statistical studies this flux is generally normalized to the reference altitude of 1000 km assuming the flux to be inversely proportional to B. At that altitude, the flux shown in Figure 3 would be 1.30×10^8. The magnitude of this flux is in good agreement with the DE 1 EICS measurements of O^+ions in the energy interval 0.01 - 1 keV during active times ($3 \leq Kp \leq 5$) in the sector 09 - 15 MLT [Yau et al., 1985].

2. O^+ Distribution in Presence of Wave-Particle Interactions

The particle trajectory calculations were then repeated with wave-particle interactions included. The wave field used for these calculations is described in Section II,2. The average fluxes of these ions in the energy and pitch-angle bins at the altitudes 4000, 8000, 12,000, 16,000, and 20,000 km are listed in Table 2. Comparison of these fluxes with those of Table 1 reveals, as expected, that the wave heating appreciably increases the energies and pitch angles of the ions. Histograms of the logarithm of the flux in shades of grey in $V_\parallel$, $V_\perp$ coordinates are shown in Figure 4. These histograms clearly show that at the higher velocities the pitch-angle distributions are conics at all altitudes. Note also that, whereas the pitch-angle distribution of the unheated ions shown in Figure 1 rapidly becomes narrower toward higher altitudes, the pitch-angle distribution of the heated ions remains broad even at the highest altitude.

Histograms of the differential omnidirectional flux, dJ/dw, at the same altitudes are shown in Figure 5. Here, note that the peak of the spectrum remaines in the lowest energy interval; it does not move toward higher energies as in the case of the unheated ions (see Figure 2). However, the spectrum becomes harder as the altitude increases.

The parallel flux and the number density of the ions as a function of height are shown in Figure 6. Both these properties are similar to those of the unheated ions shown in Figure 3. So these, too, are in agreement with the the DE 1 EICS measurements of O^+ ions in

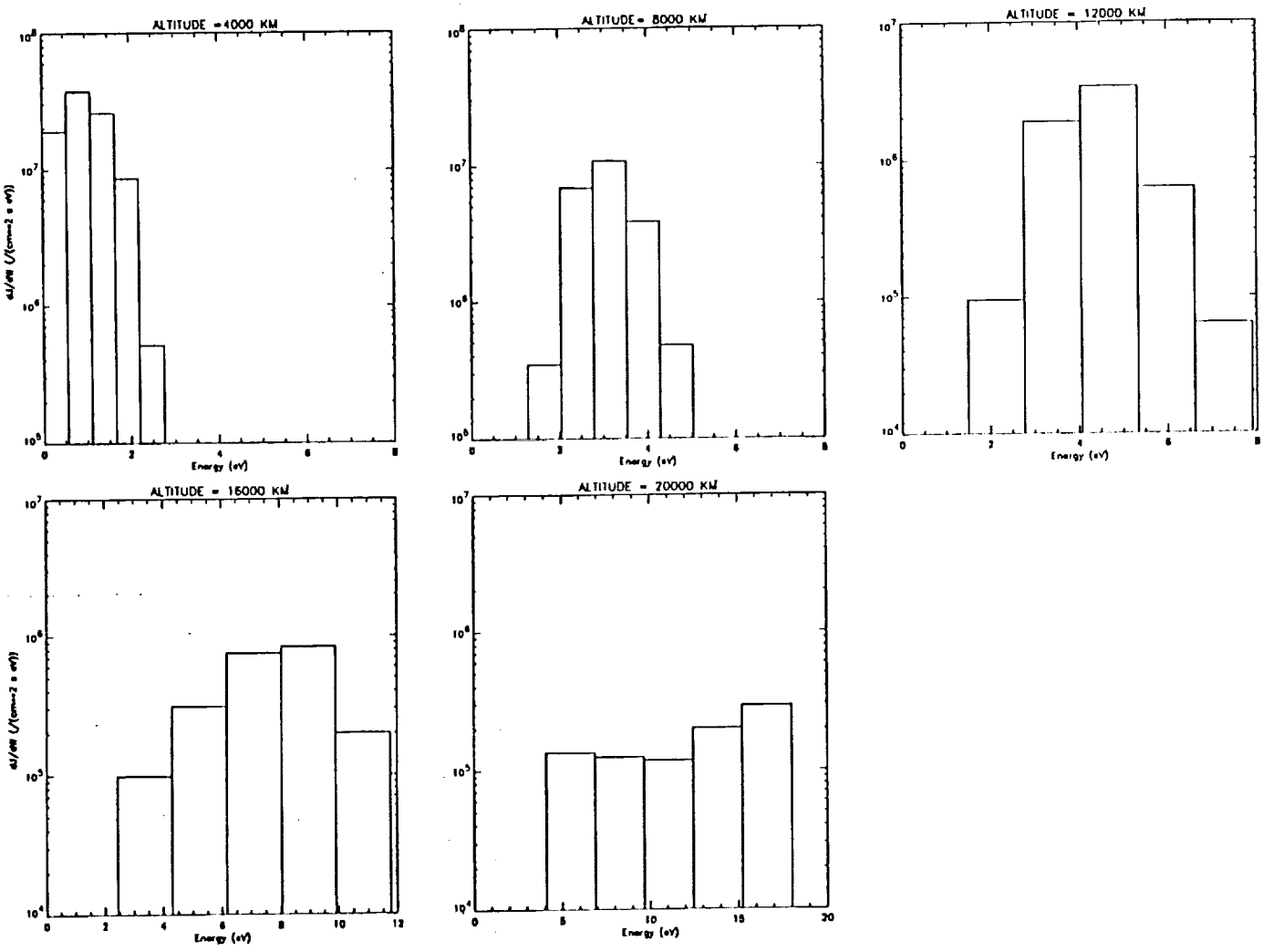

Figure 2. Omnidirectional flux of "unheated" O^+ ions versus energy. Altitudes are given at tops of graphs.

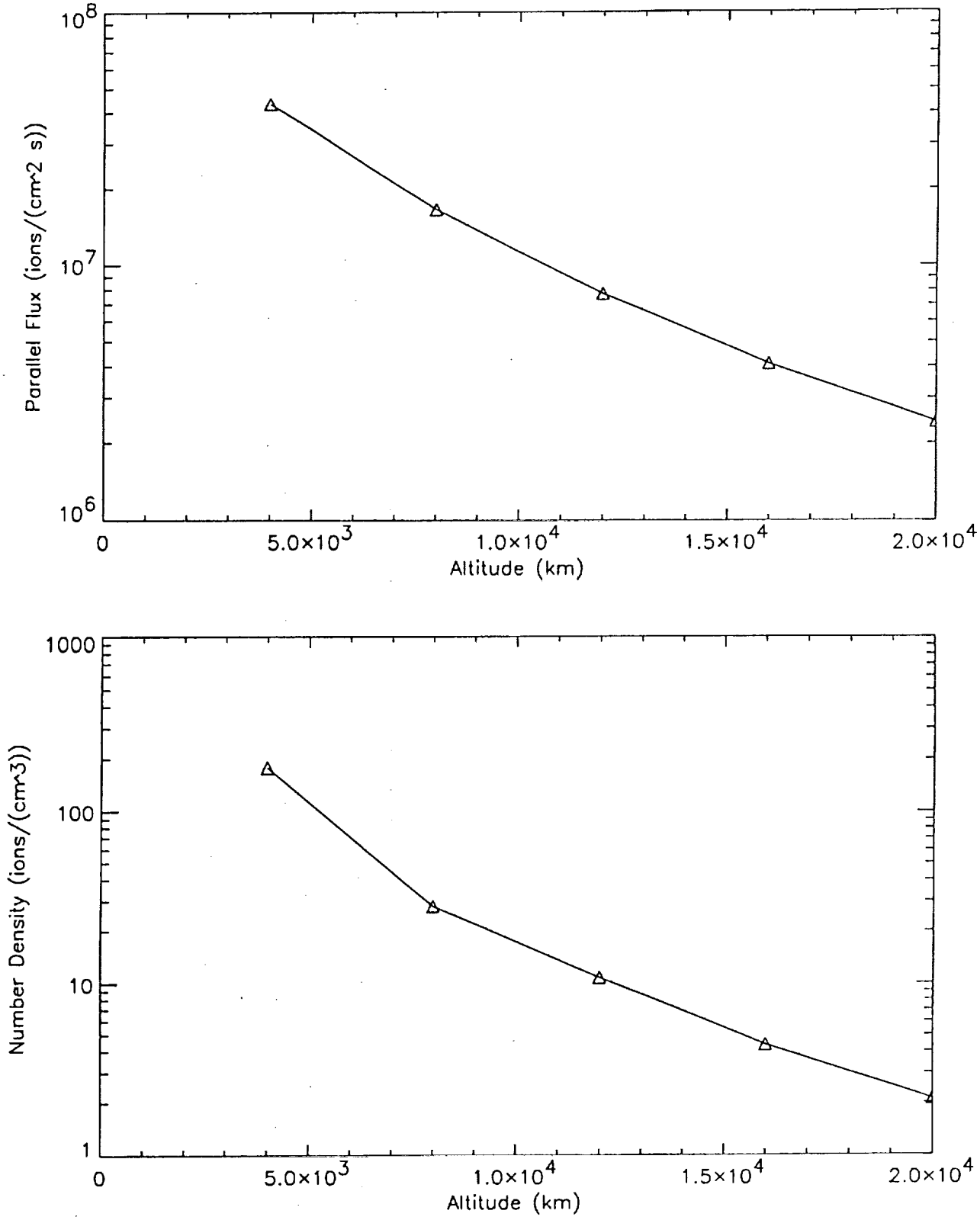

Figure 3. Parallel flux (top panel) and number density of "unheated" O^+ ions versus altitude.

Table 2. Flux ($cm^{-2}s^{-1}sr^{-1}eV^{-1}$) of "heated O^+ ions in velocity, pitch-angle bins at altitudes 4,000 to 20,000 km.

ALTITUDE = 4000 KM

Pitch-angles (deg) / Velocities (km/s)	103.96–118.78	118.78–133.61	133.61–148.43	148.43–163.26	163.26–178.08
3.87 – 22.52	2.5795E+05	2.8717E+05	1.9200E+05	2.0457E+05	8.0575E+05
22.52 – 31.61	1.4539E+05	1.0018E+05	6.5085E+03	0.0000E+00	0.0000E+00
31.61 – 38.61	5.1589E+04	5.0088E+04	0.0000E+00	0.0000E+00	0.0000E+00
38.61 – 44.53	9.3799E+03	2.0035E+04	0.0000E+00	0.0000E+00	0.0000E+00
44.53 – 49.75	1.4070E+04	1.0018E+04	0.0000E+00	0.0000E+00	0.0000E+00

ALTITUDE = 8000 KM

Pitch-angles (deg) / Velocities (km/s)	109.97–123.84	123.84–137.71	137.71–151.58	151.58–165.45	165.45–179.32
8.10 – 35.49	1.6632E+04	2.6596E+04	3.9249E+04	7.2470E+04	2.7395E+05
35.49 – 49.53	7.9831E+03	4.8850E+03	4.5506E+03	5.5140E+03	2.0444E+03
49.53 – 60.39	5.3221E+03	1.6283E+03	1.7065E+03	7.8771E+02	0.0000E+00
60.39 – 69.58	1.9958E+03	1.0856E+03	1.1377E+03	0.0000E+00	0.0000E+00
69.58 – 77.69	0.0000E+00	1.0856E+03	0.0000E+00	0.0000E+00	0.0000E+00

ALTITUDE = 12000 KM

Pitch-angles (deg) / Velocities (km/s)	109.76–123.68	123.68–137.60	137.60–151.52	151.52–165.45	165.45–179.37
10.40 – 50.47	2.5363E+03	5.6682E+03	9.7038E+03	1.5115E+04	7.4359E+04
50.47 – 70.61	3.1704E+03	9.0176E+02	9.4343E+02	3.7320E+02	4.8600E+02
70.61 – 86.16	1.1097E+03	7.7293E+02	4.0433E+02	0.0000E+00	0.0000E+00
86.16 – 99.31	0.0000E+00	1.2882E+02	0.0000E+00	0.0000E+00	0.0000E+00
99.31 – 110.91	0.0000E+00	1.2882E+02	0.0000E+00	0.0000E+00	0.0000E+00

ALTITUDE = 16000 KM

Pitch-angles (deg) / Velocities (km/s)	108.28–122.50	122.50–136.71	136.71–150.93	150.93–165.15	165.15–179.36
13.94 – 59.10	9.3798E+02	2.4306E+03	2.9413E+03	6.8091E+03	3.0318E+04
59.10 – 82.41	4.0199E+02	7.3975E+02	2.1787E+02	2.9930E+02	7.7740E+02
82.41 – 100.44	2.6799E+02	4.2271E+02	1.6340E+02	7.4825E+01	0.0000E+00
100.44 – 115.70	1.3400E+02	1.0568E+02	0.0000E+00	0.0000E+00	0.0000E+00
115.70 – 129.17	6.6998E+01	5.2839E+01	0.0000E+00	0.0000E+00	0.0000E+00

ALTITUDE = 20000 KM

Pitch-angles (deg) / Velocities (km/s)	110.51–124.33	124.33–138.15	138.15–151.98	151.98–165.80	165.80–179.62
19.21 – 62.17	4.5926E+02	1.1362E+03	1.7662E+03	3.8179E+03	1.8147E+04
62.17 – 85.80	4.9753E+02	5.6809E+02	1.6663E+02	9.3118E+01	1.1187E+03
85.80 – 104.20	1.9136E+02	2.2092E+02	9.9976E+01	0.0000E+00	0.0000E+00
104.20 – 119.81	2.2963E+02	3.1560E+01	6.6651E+01	0.0000E+00	0.0000E+00
119.81 – 133.60	3.8271E+01	1.8936E+02	0.0000E+00	0.0000E+00	0.0000E+00

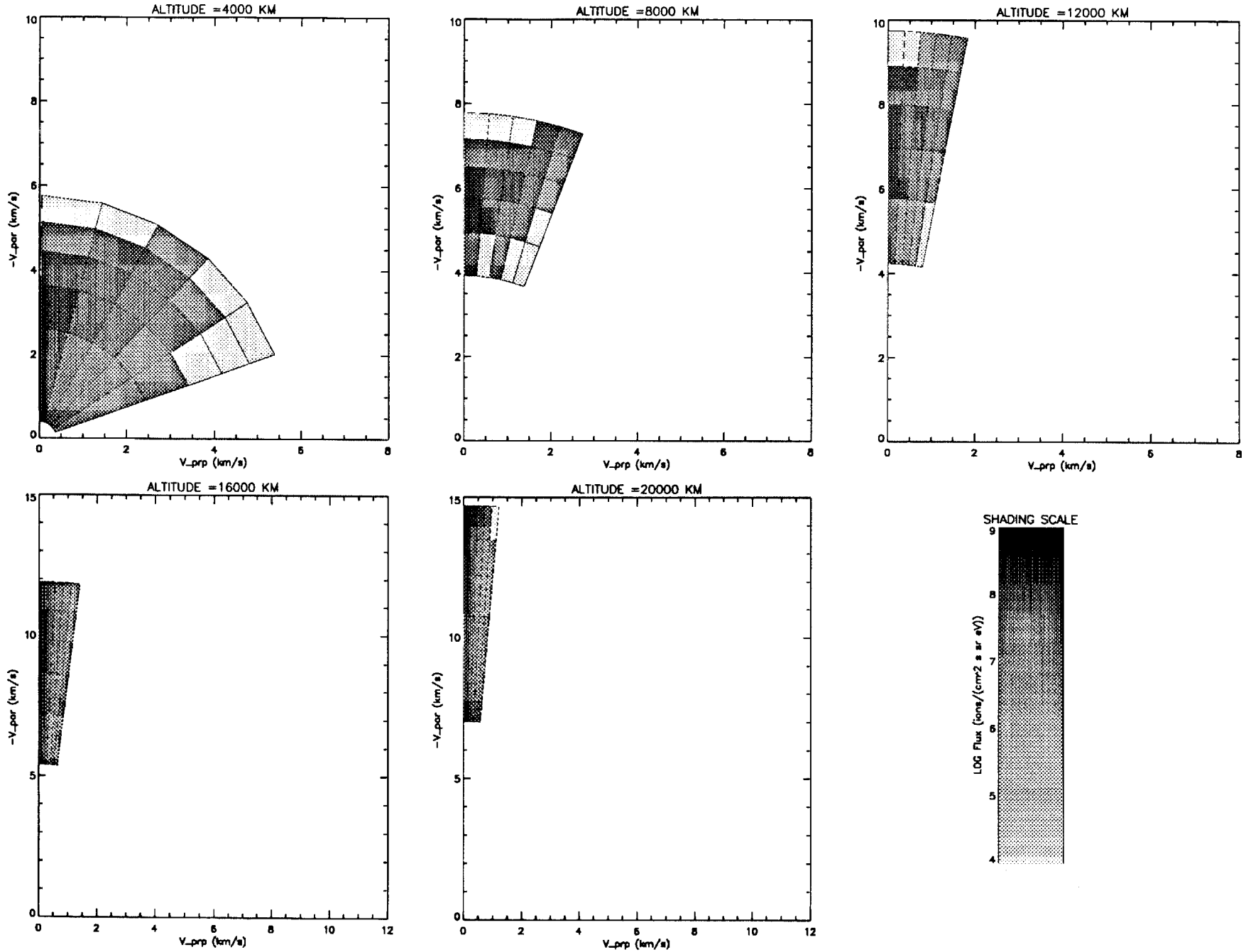

Figure 1. Flux ($cm^{-2}s^{-1}sr^{-1}eV^{-1}$) of "unheated" O^+ ions shown in shades of grey in $V_\perp$, $V_\parallel$ coordinates.

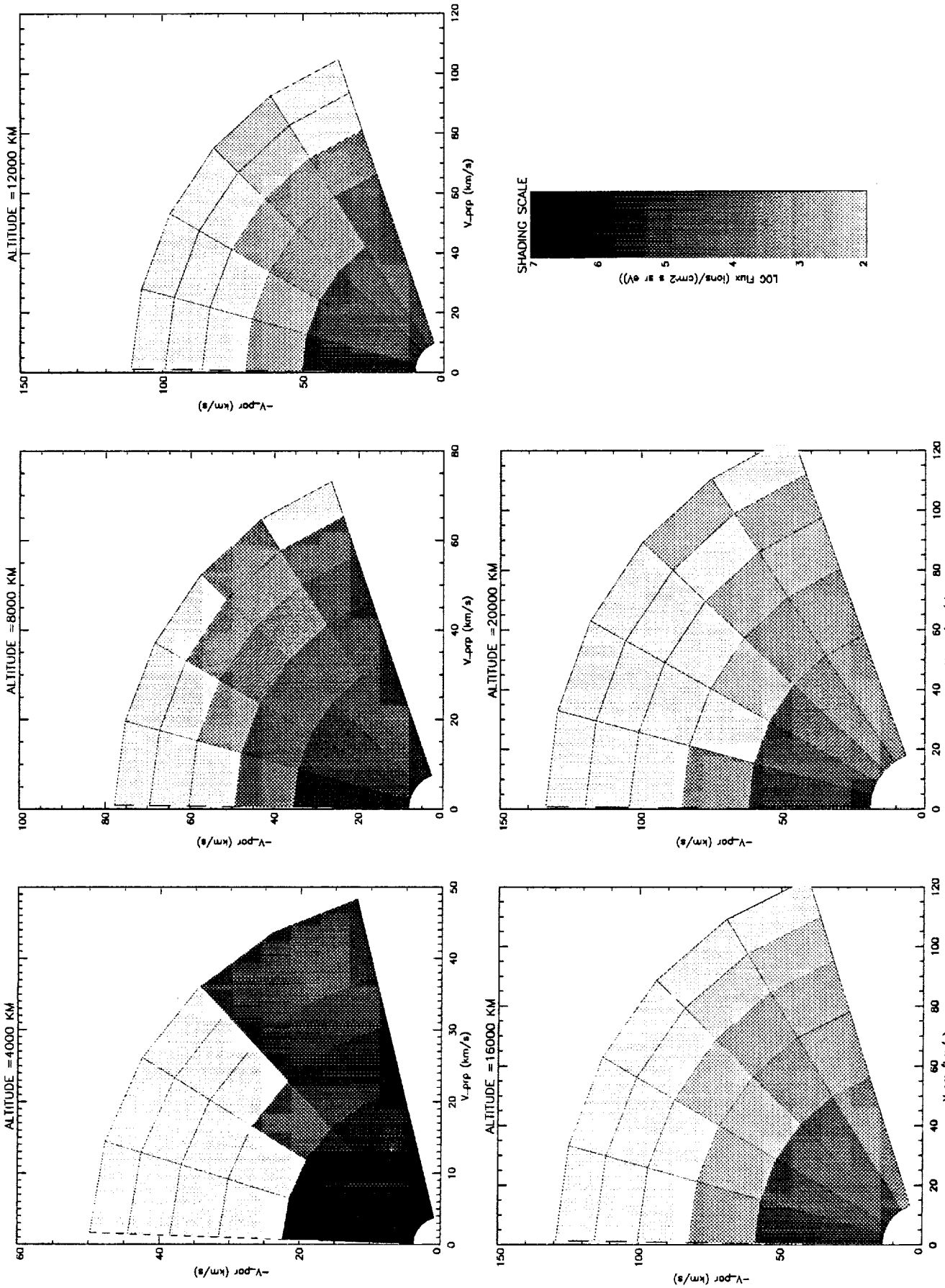

Figure 4. Flux ($cm^{-2}s^{-1}sr^{-1}eV^{-1}$) of "heated" O^+ ions shown in shades of grey in $V_\perp$, $V_\parallel$ coordinates.

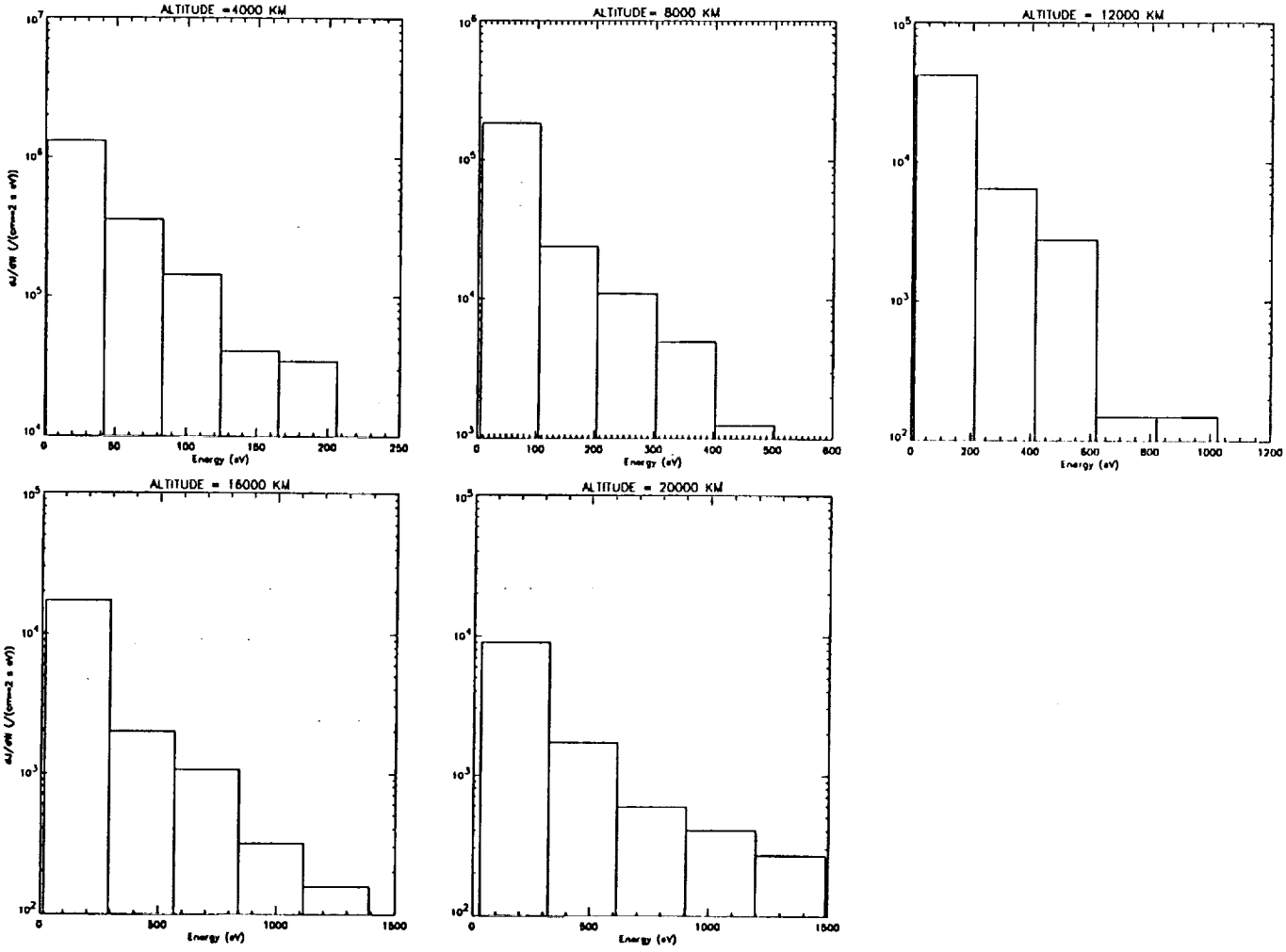

Figure 5. Omnidirectional flux of "heated" O^+ ions versus energy. Altitudes are given at tops of graphs.

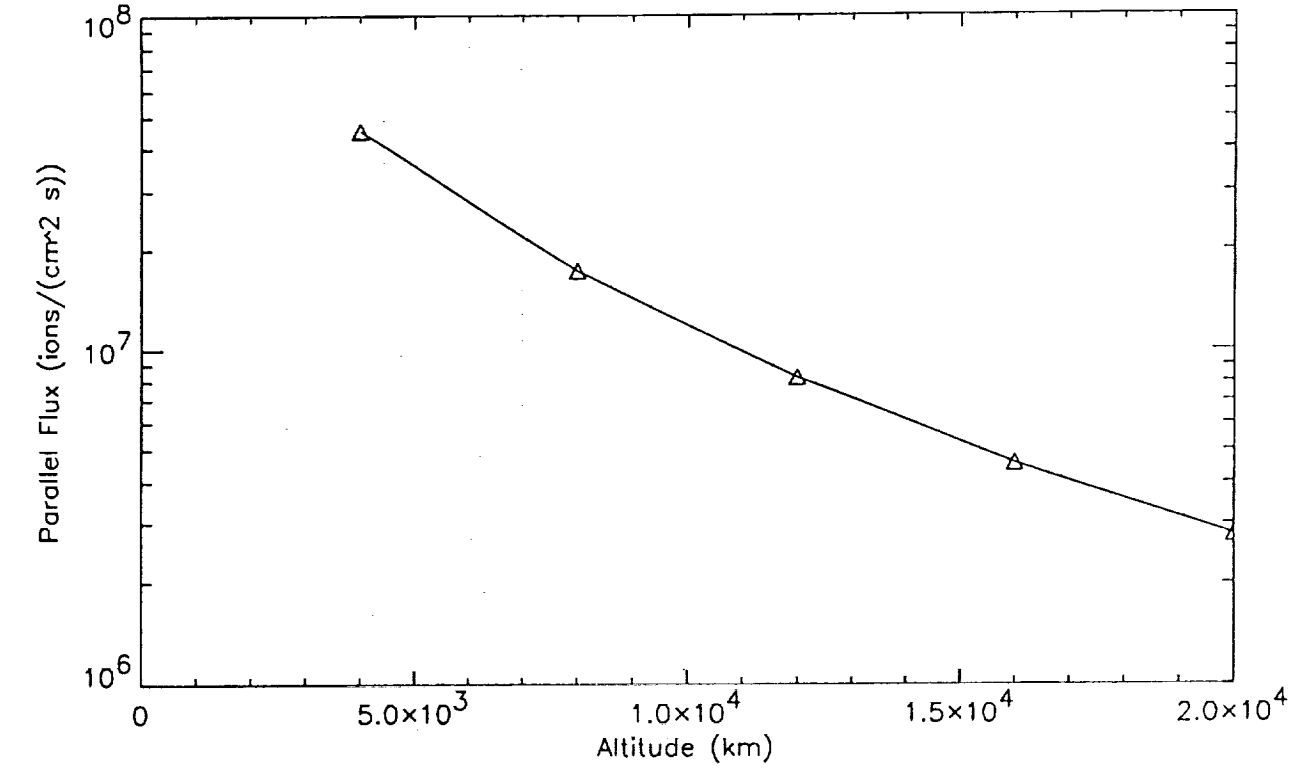

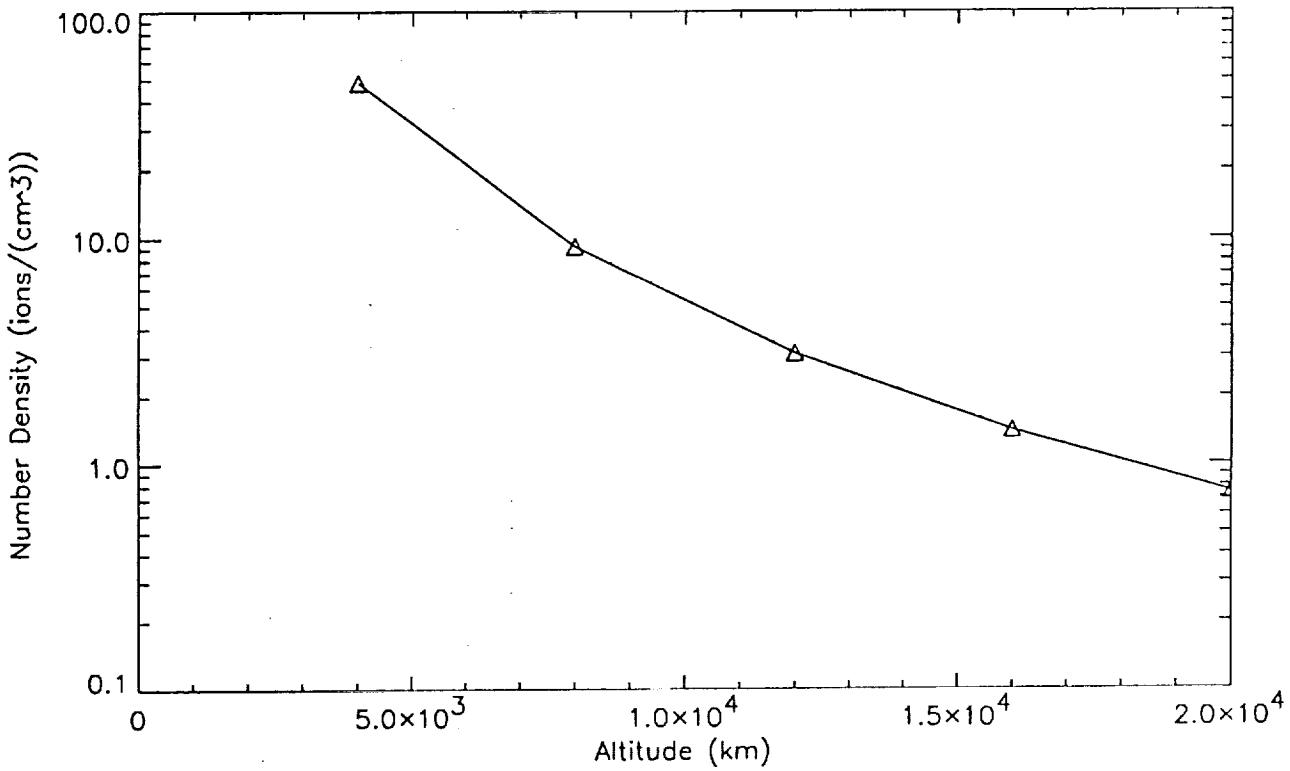

Figure 6. Parallel flux (top panel) and number density of "heated" O^+ ions versus altitude.

the energy interval 0.01 - 1 keV during active times ($3 \leq Kp \leq 5$) in the sector 09 - 15 MLT [Yau et al., 1985].

IV SUMMARY AND DISCUSSION

This study reveals that, during disturbed times, O^+ ions that are convected into the auroral zone may be accelerated along the magnetic field to velocities exceeding the gravitational escape velocity. The convection electric field, which is enhanced everywhere during disturbed times and especially in the convection throat, increases the outward flow through Joule heating in the altitude range 100 - 400 km and accelerates the ions along the magnetic field by the Coriolis force, $\vec{V}_E \cdot d\hat{e}/dt$, at all altitudes. The ions are further accelerated by the ambipolar electric field, which is enhanced principally by the precipitating electrons. The characteristics of the outflowing ions resulting from these effects are shown in Figures 1 - 3. Such upflowing-ion characteristics are similar those measured with the RIMS instrument on DE 1 [e.g., Lockwood et al., 1985; Moore et al. 1986].

Within auroral flux tubes broadband, low frequency waves are generally present [Gurnett and Frank, 1977, 1978], which accelerate ions perpendicular to the magnetic field. Thus, during the time interval that ions are convected through the auroral zone at appropriate altitudes, they become heated by the waves. The power spectral density of these waves at the resonant frequency increases with altitude, so the ion-heating rate is higher if the ions are convected through the wave region at higher altitudes. Since the convection electric field model BC of Heppner and Maynard [1987] was used in the present study, the ions remained in the auroral region during the entire time (< 1500 s) required for them to be transported from 2000 km to 20,000 km. Hence, the ions were heated continuously during this period. The resulting ion distributions due to this wave heating, in addition to the effects described above, are shown in Figures 4 - 6. Here, the spectrum of the omnidirectional flux may be characterized by a "temperature" that increases from about 21 eV at 4000 km to about 150 eV at 20,000 km. Moreover, the pitch-angle distribution remains broad at all altitudes to 20,000 km. It does not become narrower toward higher altitudes, as does the distribution of the unheated ions. Ion distributions displaying such "transversely-heated" distributions have been observed by many spacecraft at altitudes higher than about about 1 R_E. Recently, a large data base of such distributions has been obtained with the Akebono spacecraft at altitudes less than about 5000 km. The SMS instrument on this spacecraft regularly observes transitions of upflowing ions from "unheated" to "heated" distributions when the satellite enters the wave regions [Whalen et al., 1991].

Two sets of observations that substantiate these results are particularly noteworthy, those reported by André et al. [1990] and by Peterson et al. [1992]. In the former, both the "unheated" and "heated" O^+ ion populations were observed with the DE 1 satellite near 4 R_E in the cusp/cleft region. The unheated ions had energies less than 65 eV and were highly aligned with the magnetic field in the region where the wave band was narrow

and the intensity was low. In the region where the wave field was broad-band and intense, the ion distributions were similar to the one shown in Figure 4 at 20,000 km. During these observations $\vec{V}_E$ was estimated to be 5 km/s at the DE 1 altitude. In our models the value of $\vec{V}_E$ at 20,000 km was 4.64 km/s.

Peterson et al. [1992] describe simultaneous observations of upflowing ions at low and high altitudes near the same field line. One set of observations was made in the cusp/cleft region when Akebono was at an altitude of 5000 km and DE 1 was at an altitude of 21,600 km. $\vec{V}_E$ was estimated to be 7 km/s at the DE 1 altitude. The SMS instrument on Akebono measured a maximum O^+ ion flux of 2×10^5 ions/(cm^2 s sr eV), with $T_\perp \approx 10$ eV and $T_\parallel < 10$ eV. The maximum directional flux at 4000 km, in the energy interval 1.25 - 42 eV and pitch-angle range 163° - 178°, as listed in Table 2 is a factor of 4 higher than this value. Because of the viewing geometry of the SMS aperture, it is expected that the maximum flux was higher than the measured value. The perpendicular and parallel "temperatures" of the distributions are in satisfactory agreement. The EICS instrument on DE 1 measured maximum O^+ flux of 5×10^3 ions/(cm^2 s sr eV) with $T_\perp \approx 100$ eV and $T_\parallel \approx 200$ eV. The maximum directional flux at 20,000 km listed in Table 2, in the energy interval 30.7 - 322 eV and pitch-angle range 166° - 180°, is a factor of 3.6 higher than this value. The perpendicular "temperature" is approximately 100 eV, in agreement with the measurement, but the parallel "temperature" is about 140 eV, somewhat lower than the measured value. In view of the uncertainties in the model parameters used in this study, these measurements are considered to provide good support for the acceleration processes modeled in this study.

REFERENCES

Anderson, A. D., and W. E. Francis, Tables of the neutral atmosphere, in *The Trapped Radiation Handbook, DNA 2524H*, ed. by J.B. Cladis, G.T. Davidson, and L.L. Newkirk, The Defense Nuclear Agency, Washington, D.C., 1971.

André, M., G.B. Crew, W.K. Peterson, A.M. Persoon, C.J. Pollock, and M.J. Engebretson, Ion heating by broadband low-frequency waves in the cusp/cleft, *J. Geophys. Res., 95*, 20809, 1990.

Chandrasekhar, S., *Principles of Stellar Dynamics*, p.89, University of Chicago Press, Chicago, 1942.

Chiu, Y.T., J.B. Cladis, and W.E. Francis, Simulation of ion heating in the topside auroral ionosphere, *Geophys. Res. Lett., 15*, 1534, 1988.

Cladis, J.B., Parallel acceleration and transport of ions from polar ionosphere to plasma sheet, *Geophys. Res. Lett., 13*, 893, 1986.

Cladis, J.B., Transport of ionospheric ions in the magnetosphere: theory and observations, *Adv. Space Res., Vol. 8, No. 8*, 165, 1988.

Cladis, J.B., and W.E. Francis, The polar ionosphere as a source of the storm time ring current, *J. Geophys. Res., 90*, 3465, 1985.

Cladis, J.B., and W.E. Francis, Distribution in magnetotail of O^+ ions from cusp/cleft ionosphere: LA possible substorm trigger, *J. Geophys. Res., 97*, 123, 1992.

Crew, G.B., T. Chang, J.M. Retterer, W.K. Peterson, D.A. Gurnett, and R.L. Huff, Ion cyclotron resonance heated conics: theory and observations, *J. Geophys. Res. 95*, 3957, 1990.

Delcourt, D.C., J.A. Sauvaud, and T.E. Moore, Cleft contribution to ring current formation, *Jour. Geophys. Res. 95*, 20,937, 1990.

Gambosi, T.I., and T.L. Killeen, Effects of thermospheric motions on the polar wind: A time-dependent numerical study, J. Geophys. Res., 92, 4725, 1987.

Gurnett, D.A., and L.A. Frank, A region of intense plasma wave turbulence on auroral field lines, J. Geophys. Res., 82, 1031, 1977.

Gurnett, D.A., R.L. Huff, J.D. Menietti, J.L. Burch, J.D. Winningham, and S.D. Shawhan, Correlated low-frequency electric and magnetic noise along auroral field lines, J. Geophys. Res., 89, 8971, 1984.

Heppner, J. P., and N. C. Maynard, Empirical high-latitude electric field models, *J. Geophys. Res. 92*, 4467, 1987.

Horwitz, J.L., Core plasma in the magnetosphere, *Rev. Geophys., 25*, 579, 1987.

Kintner Jr., P.M., Observations of velocity shear driven plasma turbulence, *J. Geophys. Res., 81*, 5114, 1976.

Lockwood, M., J.H. Waite, Jr., T.E. Moore, J.F.E. Johnson, and C.R. Chappell, A new source of suprathermal O^+ions near the dayside polar cap boundary, *J. Geophys. Res., 90*, 4099, 1985.

Moore, T.E., M. Lockwood, M.O. Chandler, J.H. Waite, Jr., C.R. Chappell, A. Persoon, and M. Sugiura, Upwelling O^+ion source characteristics, *J. Geophys. Res., 91*, 7019, 1986.

Northrop, T.G., *The Adiabatic Motion of Charged Particles*, Wiley- Interscience, New York, 1963.

Peterson, W.K., E.G. Shelley, J.H. Waite, Jr., and T.E. Moore, Observations of simultaneous bulk heating and tail energization of ionospheric oxygen, *EOS, Trans. Am. Geophys. Union, 67*, 1134, 1986.

Peterson, W.K., A.W. Yau, and B.A. Whalen, Simultaneous observations of H^+ and O^+ ions at two altitudes by the Akebono and Dynamics Explorer-1 satellites, Heppner, *J. Geophys. Res., to appear, 1992.*

Sandholt, P. E., Polar cusp electrodynamics — a case study, in *Modeling Magnetospheric Plasma*, p 191, ed by T. E. Moore and J. H. Waite, Jr., Geophys. Monograph 44, American Geophysical Union, Washington, D. C., 1988.

Sandholt, P. E., B. Jacobsen, B. Lybekk, A. Egeland, P. F. Bythrow, and D. A. Hardy, Electrodynamics of the polar cusp ionosphere; A case study, *J. Geophys. Res., 94*, 6713, 1989a.

Sandholt, P. E., B. Jacobsen, B. Lybekk, A. Egeland, C.-I. Meng, P. T. Newell, F. J. Rich, and E. J. Weber, *J. Geophys. Res., 94*, 8928, 1989b.

Spitzer Jr., L., *Physics of Fully Ionized Gases*, p. 65, Interscience Publishers Ltd, London, 1956.

Sugiura, M., T. Iyemori, R. A. Hoffman, N. C. Maynard, J. L. Burch, and J. D. Winningham, Relationships between field-aligned currents, electric fields, and particle precipitation as observed by Dynamics Explorer-2, in *Magnetospheric Currents, Geophys. Monogr. Ser., Vol. 28*, edited by T. A. Potemra, p. 96, AGU, Washington, D. C., 1984.

Tsyganenko, N. A., Global quantitative models of the geomagnetic field in the cislunar magnetosphere for different disturbance levels, *Planet. Space Sci., 35*, 1347, 1987.

Whalen, B.A., S. Watanabe, and A.W. Yau, Observation in the Transverse ion energization region, *Geophys. Res. Lett. 18*, 725, 1991.

Yau, A.W., E.G. Shelley, W.K. Peterson, and L. Lenchyn, Energetic auroral and polar ion outflow at DE 1 Altitudes: Magnitude, composition, magnetic activity dependence, and long-term variations, *J. Geophys. Res., 90*, 8417, 1985. Yau, A.W., E.G. Shelley, and W.K. Peterson, Accelerated auroral and polar-cap ions: Outflow at DE-1 altitudes, pp. 72-76, in *Ion Acceleration in the Magnetosphere and Ionosphere*, edited by T. Chang, Geophysical Monograph, 38, 1986.

Yau, A.W., W.K. Peterson, and E.G. Shelley, Quantitative parametrization of energetic ionospheric ion outflow, *Modeling Magnetospheric Plasma, ed. by T.E. Moore and J.H. Waite, Jr., Geophysical Monograph 44*, p 211, 1988.

Yau, A.W., and M. Lockwood, Vertical ion flow in the polar ionosphere, *Modeling Magnetospheric Plasma, ed. by T.E. Moore and J.H. Waite, Jr., Geophysical Monograph 44*, p 229, 1988.

REPORT DOCUMENTATION PAGE

Form Approved
OMB No. 0704-0188

1. AGENCY USE ONLY *(Leave blank)*	2. REPORT DATE	3. REPORT TYPE AND DATES COVERED
	8-7-92	CR 8-7-92

4. TITLE AND SUBTITLE
Effects of Convection Electric Field on Upwelling and Escape of Ionospheric O+

5. FUNDING NUMBERS
NAS5-31211

6. AUTHOR(S)
J.B. Cladis, Yam T. Chiu and William K. Peterson

7. PERFORMING ORGANIZATION NAME(S) AND ADDRESS (ES)
Lockheed Palo Alto Research Laboratory
3251 Hanover St.
Palo Alto, CA 94304

8. PEFORMING ORGANIZATION REPORT NUMBER
CR189298

9. SPONSORING / MONITORING ADGENCY NAME(S) AND ADDRESS (ES)
National Aeronautics and Space Administration
Goddard Space Flight Center, Greenbelt, MD 20771

10. SPONSORING / MONITORING ADGENCY REPORT NUMBER
CR189298

11. SUPPLEMENTARY NOTES

12a. DISTRIBUTION / AVAILABILITY STATMENT
Not Given

12b. DISTRIBUTION CODE

13. ABSTRACT *(Maximum 200 words)*

A Monte Carlo code used to explore effects of convection electric field on O+ ions from cusp/cleft ionosphere. Trajectories of individual ions/neutrals computed as they undergo charge-exchange collisions. In ion state, trajectories computed in realisitc models of magnetic field and the convection, corotation and ambipolar electric fields. Effects of collisions are included, and trajectories computed with/without simultaneous stochastic heating perpendicular to magnetic field by model of broadband, low frequency waves. In neutral state, ballistic trajectories in gravitational field are computed. Initial conditions of ions were obtained from Gombose and Killeen [1987], who used hydrodynamic code to simulate time-dependent frictional-heating effects in magnetic tube during motion through the convection throat. Distribution of ion fluxes as function of height are constructed. Results show high flux of low-energy O+ ions flow outward from ionosphere, reach energies approaching 15 e V, pitch-angle narrow. If ions enter region of broadband low-frequency wave field, they become heated, energy increases and pitch-angle broadens. Further result strong electric fields perpendicular to magnetic field in cusp/cleft auroral structures can accelerate O+ ions from ionosphere, even in absence of heating and diffusion. Ion with initial energy of 0.6 eV and pitch-angle 45% at 2000 km is accelerated to 105 eV at 20,000 km if within magentic field lines.

14. SUBJECT TERMS
Convection, O+ ions, cusp/cleft ionosphere, ballistic trajectories, broadband, ambipolar electric field, Gombose/Killeen, Sugiura et al, Sandholt & Sandholt, equipotentials

15. NUMBER OF PAGES
App. 50

16. PRICE CODE

17. SECURITY CLASSIFICATION OF REPORT	18. SECURITY CLASSIFICATION OF THIS PAGE	19. SECURITY CLASSIFICATION OF ABSTRACT	20. LIMITATION OF ABSTRACT
Unclassified	Unclassified	Unclassified	UL